REPORT SD-TR-88-99

Ion Mixing of Ti and TiO_y Films on SiO_x

Prepared by

A. A. GALUSKA, J. C. UHT, P. M. ADAMS and J. M. COGGI
Materials Sciences Laboratory
Laboratory Operations
The Aerospace Corporation
El Segundo, CA 90245

4 November 1988

Prepared for

SPACE DIVISION
AIR FORCE SYSTEMS COMMAND
Los Angeles Air Force Base
P.O. Box 92960
Los Angeles, CA 90009-2960

This report was submitted by The Aerospace Corporation, El Segundo, CA 90245, under Contract No. F04701-85-C-0086-P00016 with the Space Division, P.O. Box 92960, Los Angeles, CA 90009-2960. It was reviewed and approved for The Aerospace Corporation by R. W. Fillers, Director, Materials Sciences Laboratory.

Lt Constance M. Chintall/CNCIV was the project officer for the Mission-Oriented Investigation and Experimentation (MOIE) Program.

This report has been reviewed by the Public Affairs Office (PAS) and is releasable to the National Technical Information Service (NTIS). At NTIS, it will be available to the general public, including foreign nationals.

This technical report has been reviewed and is approved for publication. Publication of this report does not constitute Air Force approval of the report's findings or conclusions. It is published only for the exchange and stimulation of ideas.

for CONSTANCE M. CHINTALL, Lt, USAF
MOIE Project Officer
SD/CNCIV

RAYMOND M. LEONG, Maj, USAF
Deputy Director, AFSTC West Coast Office
AFSTC/WCO OL-AB

UNCLASSIFIED

SECURITY CLASSIFICATION OF THIS PAGE

REPORT DOCUMENTATION PAGE

1a. REPORT SECURITY CLASSIFICATION Unclassified	1b. RESTRICTIVE MARKINGS
2a. SECURITY CLASSIFICATION AUTHORITY	3. DISTRIBUTION / AVAILABILITY OF REPORT Approved for public release; distribution unlimited.
2b. DECLASSIFICATION / DOWNGRADING SCHEDULE	
4. PERFORMING ORGANIZATION REPORT NUMBER(S) TR-0086A(2935-12)-4	5. MONITORING ORGANIZATION REPORT NUMBER(S) SD-TR-88-99
6a. NAME OF PERFORMING ORGANIZATION The Aerospace Corporation Laboratory Operations 6b. OFFICE SYMBOL (If applicable)	7a. NAME OF MONITORING ORGANIZATION Space Division
6c. ADDRESS (City, State, and ZIP Code) El Segundo, CA 90245	7b. ADDRESS (City, State, and ZIP Code) Los Angeles Air Force Base Los Angeles, CA 90009-2960
8a. NAME OF FUNDING / SPONSORING ORGANIZATION 8b. OFFICE SYMBOL (If applicable)	9. PROCUREMENT INSTRUMENT IDENTIFICATION NUMBER F04701-85-C-0086 -P00016
8c. ADDRESS (City, State, and ZIP Code)	10. SOURCE OF FUNDING NUMBERS PROGRAM ELEMENT NO. / PROJECT NO. / TASK NO / WORK UNIT ACCESSION NO.

11. TITLE (Include Security Classification)
Ion Mixing of Ti and TiO_y Films on SiO_x

12. PERSONAL AUTHOR(S)
Galuska, A. A., Uht, J. C., Adams, P. M., and Coggi, J. M.

13a. TYPE OF REPORT	13b. TIME COVERED FROM ____ TO ____	14. DATE OF REPORT (Year, Month, Day)	15. PAGE COUNT
		1988 November 4	28

16. SUPPLEMENTARY NOTATION

17. COSATI CODES		
FIELD	GROUP	SUB-GROUP

18. SUBJECT TERMS (Continue on reverse if necessary and identify by block number)
Ion Implantation, Interfacial Mixing, Spectroscopy, Titanium oxides, X-ray Diffraction, Silicon oxides, Auger

19. ABSTRACT (Continue on reverse if necessary and identify by block number)

The influence of ion implantation on the interfacial chemistry, morphology, and adhesion of Ti and TiO_y films on SiO_x was examined. The Ti/SiO_x and TiO_y/SiO_x specimens were implanted with varying doses of $^{84}Kr^+$ at different substrate temperatures (2×10^{16} Kr/cm^2 at 70°C, 1×10^{17} Kr/cm^2 at 70°C, and 1×10^{17} Kr/cm^2 at 350°C). These $^{84}Kr^+$-implanted specimens were compared to specimens vacuum annealed at 1000°C for 3600 s. Ion implantation intermixed interfacial Ti, Si, and O in both the Ti/SiO_x and TiO_y/SiO_x specimens, producing interfacial Ti-Si oxide layers. This interfacial mixing increased with both implantation dose and

20. DISTRIBUTION / AVAILABILITY OF ABSTRACT	21. ABSTRACT SECURITY CLASSIFICATION
☒ UNCLASSIFIED/UNLIMITED ☐ SAME AS RPT. ☐ DTIC USERS	Unclassified
22a. NAME OF RESPONSIBLE INDIVIDUAL	22b. TELEPHONE (Include Area Code) / 22c. OFFICE SYMBOL

DD FORM 1473, 84 MAR 83 APR edition may be used until exhausted. All other editions are obsolete.

SECURITY CLASSIFICATION OF THIS PAGE
UNCLASSIFIED

19. ABSTRACT (Continued)

temperature. Despite similar interfacial mixing, the influence of ion implantation on film adhesion was very different for the Ti/SiO_x and TiO_y/SiO_x specimens. Ion implantation promoted Si-O-Ti bonding at the Ti/SiO_x interface, resulting in a 10-fold adhesion increase. In contrast, ion implantation did not enhance the adhesion of the TiO_y films. The implanted $^{84}Kr^+$ coalesced in both the Ti/SiO_x and TiO_y/SiO_x specimens, resulting in void, bubble, and crack formation. Film characterization was performed using Rutherford backscattering spectrometry, Auger electron spectroscopy, X-ray photoelectron spectroscopy, scanning electron microscopy, and X-ray diffraction. Film adhesion was examined using a scratch test.

PREFACE

The authors are grateful to L. Crocko and S. Hornung for their assistance with the ion implantation and the AES/XPS analyses, respectively. The AES and XPS analyses were performed at the Analytical Service Center of the American Hospital Supply Corporation, Irvine, California. Ion implantation was performed at Kroko Engineering, Tustin, California. This work was supported by The Aerospace Corporation Mission Oriented Investigation and Experimentation program.

CONTENTS

FIGURES

TABLES

I. INTRODUCTION

Interfacial properties are often difficult to control using conventional deposition and thermal processing techniques. Ion mixing has potential for modifying these interfacial properties in previously unattainable ways.[1-5] In particular, ion mixing has been used rather extensively to enhance the adhesion between thin films and substrates. Ion mixing can increase thin film adhesion by inducing interfacial compound formation, by mechanically interlocking film and substrate, and by grading the interface between film and substrate.[6-9] Most investigations of ion-induced adhesion enhancement have dealt with metal films on oxide, polymer, semiconductor, and metal substrates.[10-12] Interfacial mixing, reaction, and adhesion enhancement are usually extensive when the film and substrate are exothermically reactive.[11] In contrast, interfacial mixing, reaction, and adhesion enhancement are usually minimal when the film and substrate are endothermically reactive.[11,12]

The potential of ion mixing for modifying the interfacial properties of metal oxide films on metal oxide substrates has yet to be adequately determined. The extent of ion-induced interfacial mixing is difficult to predict because most oxide-oxide reactions are neither highly exothermic nor highly endothermic. In addition, it is unclear whether ion mixing will promote the formation of glassy oxide mixtures or whether the oxide phases will separate. Both of these factors will have a large influence on the adhesion enhancement expected from ion mixing.

In this study, we investigated the influence of ion mixing on the interfacial properties of TiO_y and Ti films on SiO_x. The interactions of Ti and TiO_y with SiO_x are very different thermodynamically. The reduction-oxidation reaction between Ti and SiO_2 is highly exothermic ($2Ti + SiO_2 \rightarrow Si + 2TiO$; $\Delta G_f^\circ = -167$ kJ-mole^{-1} at 25°C). In contrast, TiO_2 and SiO_2 do not react to form a new product. They may be intermixed in a glassy form, but separate into discrete phases upon crystallization.[13] The ion-induced interfacial chemistry, morphology, and adhesion modifications produced in the Ti/SiO_x and TiO_y/SiO_x specimens are discussed in terms of the thermodynamic properties of the films.

II. EXPERIMENTAL

The substrates used in our studies were n-type Czochralski silicon wafers with a <100> orientation. The wafers were steam oxidized at 925°C to produce SiO_x ($SiO_{2.2}$ as determined by Rutherford backscattering analysis) layers approximately 1300 Å thick. Prior to deposition the wafers were cleaned with trichloroethane, methanol, and deionized water. Titanium and titanium dioxide films 400 Å thick were deposited using magnetron sputtering with ultra-pure argon (99.999%) and a base pressure of 5×10^{-7} Torr. These films were implanted with $^{84}Kr^{+}$ using a Varian Extrion 200-A2F ion implanter. The Extrion 200-A2F was equipped with a variable temperature stage heated by quartz halogen lamps. The samples were clipped to this implanter stage during implantation. Sample temperature was calibrated against stage temperature and the implant power density by placing iron-constantan thermocouples against the stage and the backside of a test sample during implantation at various power densities and stage temperatures. The $^{84}Kr^{+}$ implants were performed using a 180 keV ion beam with a current density of 2.5 $\mu A\text{-}cm^{-2}$. Krypton implantation was performed at the following doses and temperatures: 5×10^{16} $Kr\text{-}cm^{-2}$ at 70°C, 1×10^{17} $Kr\text{-}cm^{-2}$ at 70°C, and 1×10^{17} $Kr\text{-}cm^{-2}$ at 350°C. The ion beam energies were chosen in order to place the implantation peaks just beyond the critical interfaces.

Several of the as-deposited specimens were exposed to thermal treatments in order to compare the influence of thermal and ion processing. Thermal treatments were performed using a vacuum furnace. The furnace was pumped down to 5×10^{-7} Torr using an oil diffusion pump. The specimens were then heated to 1000°C for 3600 s.

The mixing process was examined using Rutherford backscattering spectrometry (RBS) and Auger electron spectroscopy (AES). The RBS measurements were obtained on a General Ionex Tandetron Model 4110A using 3.0 MeV He^{++} ions. Specimens were tilted by 70° to improve depth resolution. AES analyses were obtained from a Perkin-Elmer PHI Multiprobe 6000 scanning Auger spectrometer using a 5.0 keV electron beam. Sputter depth profiling was performed using a 3.0 keV Ar^{+} ion beam. Crystallite identification was determined using X-ray

diffraction (XRD) with a Read camera (glancing 15° angle) and Cu Kα radiation. The diffracted X-ray intensities were very low. As a result, X-ray exposures of 5.76×10^4 s were required. Analysis was performed under vacuum (~ 1×10^{-3} Torr) to minimize atmospheric scattering of the diffracted radiation. The chemical state of the films was examined with a Perkin-Elmer PHI 5400 X-ray photoelectron spectrometer (XPS) using Mg Kα radiation. The C 1s peak of adventitious carbon was used for energy calibration. This calibration gave Si 2p peaks at 103.3 and 99.0 eV for SiO_2 and metallic Si, respectively. Sputter erosion and cleaning was performed using a 1 keV Ar^+ ion beam. Ion sputtering resulted in the reduction of the TiO_2 films to TiO and Ti_2O_3, but had no apparent influence on the SiO_2 films.[14] Topographical changes and corresponding elemental compositions were determined using a Jeol JSM-840 scanning electron microscope (SEM) equipped with a Philips EDAX 9900 energy dispersive X-ray (EDX) system.

The adherence of the as-deposited and processed films was examined using a scratch test.[15,16] Scratch testing was performed on a Wilson Instruments Tukon microhardness tester using a 136° Knoop diamond indenter. Loads between 1 and 200 grams were applied to the indenter, which was manually drawn across the sample surface at ~ 0.2 mm-s^{-1}. The minimum load necessary to remove a film from its substrate was used as a measure of the film adhesion. Scratches were examined by SEM to determine at what loads the films began to detach. EDX analysis was used to confirm the complete removal of the films from the scratches. The precision of these measurements was approximately 20% relative standard deviation for loads above 10 g.

III. RESULTS AND DISCUSSION

A. $Ti/SiO_x/Si$

The as-deposited Ti films were composed of α- and β-Ti (see Fig. 1), and appeared smooth under SEM examination at 20,000X magnification. The RBS spectrum in Fig. 1a shows that the interface between the Ti and SiO_x was discrete. The Ti films contained high concentrations of oxygen, which were incorporated during deposition and subsequent exposure to atmosphere. This oxygen concentration varied from ~ 47 atomic percent at the surface to ~ 16 atomic percent at the Ti/SiO_x interface. As shown in Fig. 1b, vacuum annealing at 1000°C for 3600 s enhanced the reduction of the SiO_x by the Ti film. The solubility of O in crystalline Ti is rather high (~ 30 atomic percent). As a result, the oxygen that was liberated from the SiO_x layer was able to diffuse throughout the entire Ti film. Silicon, which diffuses very slowly in SiO_2 and is insoluble in crystalline TiO_2, showed no redistribution upon annealing. XRD analysis (see Table 1) of the annealed specimens showed the presence of monoclinic TiO. The surface topography of the as-deposited specimens was unaffected by the anneal.

Ti/SiO_x specimens were implanted with $^{84}Kr^+$ to determine the influence of ion dose and implantation temperature on specimen chemistry and morphology. Krypton implants were performed to 2×10^{16} Kr-cm^{-2} at 70°C, 1×10^{17} Kr-cm^{-2} at 70°C, and 1×10^{17} Kr-cm^{-2} at 350°C. The 2×10^{16} Kr-cm^{-2} implant had no influence on the surface topography of the Ti/SiO_x specimens. Increasing the dose to 1×10^{17} Kr-cm^{-2} resulted in krypton coalescence in the SiO_x layers. This coalescence produced a high density of voids and also surface bubbles on these $^{84}Kr^+$ implanted specimens. An example of this voided surface topography is shown in Fig. 2. Implantation temperature had no influence on the observed surface topography.

RBS spectra of the $^{84}Kr^+$-implanted specimens are compared in Fig. 3. These RBS spectra show that approximately 50% of the implanted $^{84}Kr^+$ passed through the Ti/SiO_x interface. As with thermal processing, the 2×10^{16} Kr-cm^{-2} implant enhanced the reduction of the SiO_x layer and the diffusion of O throughout the Ti film. However, unlike thermal processing, ion bombardment

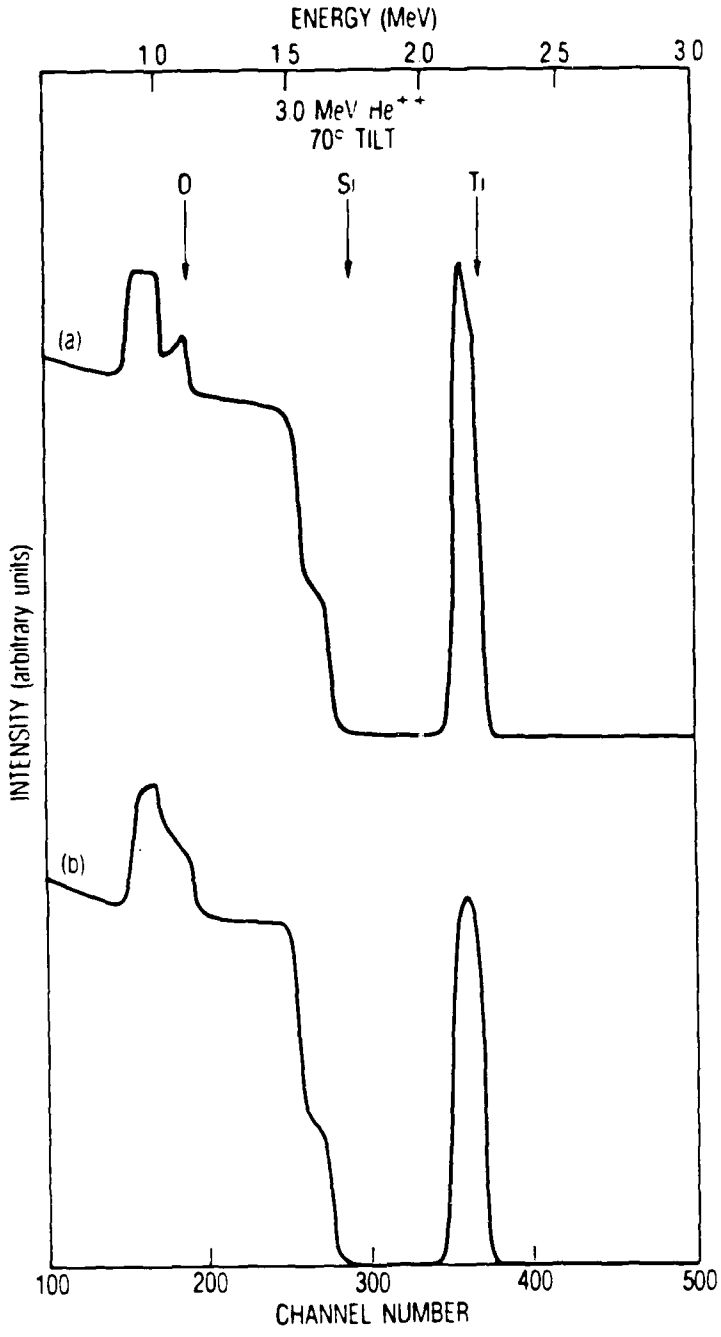

Fig. 1. RBS Spectra of As-Deposited and Thermally Processed Ti/SiO_x Specimens. (a) As-Deposited specimen; (b) specimen vacuum annealed for 3600 s at 1000°C.

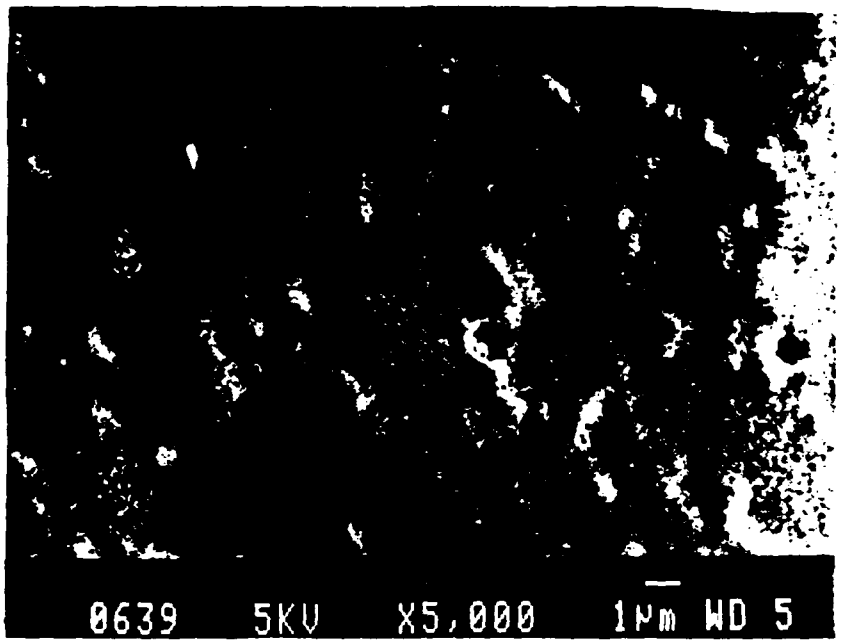

Fig. 2. SEM Micrograph of a Ti/SiO_x Specimen, Following Implantation with 1×10^{17} Kr-cm^{-2} at 70°C. Micrometer sized bubbles and submicron sized voids are apparent.

also induced the intermixing of interfacial Si and Ti. The resulting Ti film had an average stoichiometry of approximately $TiO_{0.9}Si_{0.3}$. As expected for an ion-induced process, the gettering of O into the Ti film from the underlying SiO_x (also from the ambient above the specimen surface) increased substantially when the implant dose was increased to 1×10^{17} Kr-cm^{-2} at 70°C. Similarly, the quantity of Ti mixed into the SiO_x layer increased with ion dose. In contrast, the quantity of Si mixed into the Ti film decreased. Ion mixing had lowered the miscibility of Si in the Ti film. This trend continued as the implantation temperature was increased to 350°C. As shown in Fig. 3d, the rise in temperature increased the gettering of O into the Ti film and the redistribution of Ti into the SiO_x underlayer. However, the Si content (also the Kr content) of the Ti film decreased. These elemental redistributions transformed the Ti film into $TiO_{2.3}$ and the SiO_x layer into a mixed Ti-Si oxide layer, grading from the Si substrate to the $TiO_{2.3}$ film. In addition to Ti/SiO_x intermixing, a small quantity of the implanted $^{84}Kr^+$ reached the SiO_x/Si interface, producing a graded O distribution at that interface.

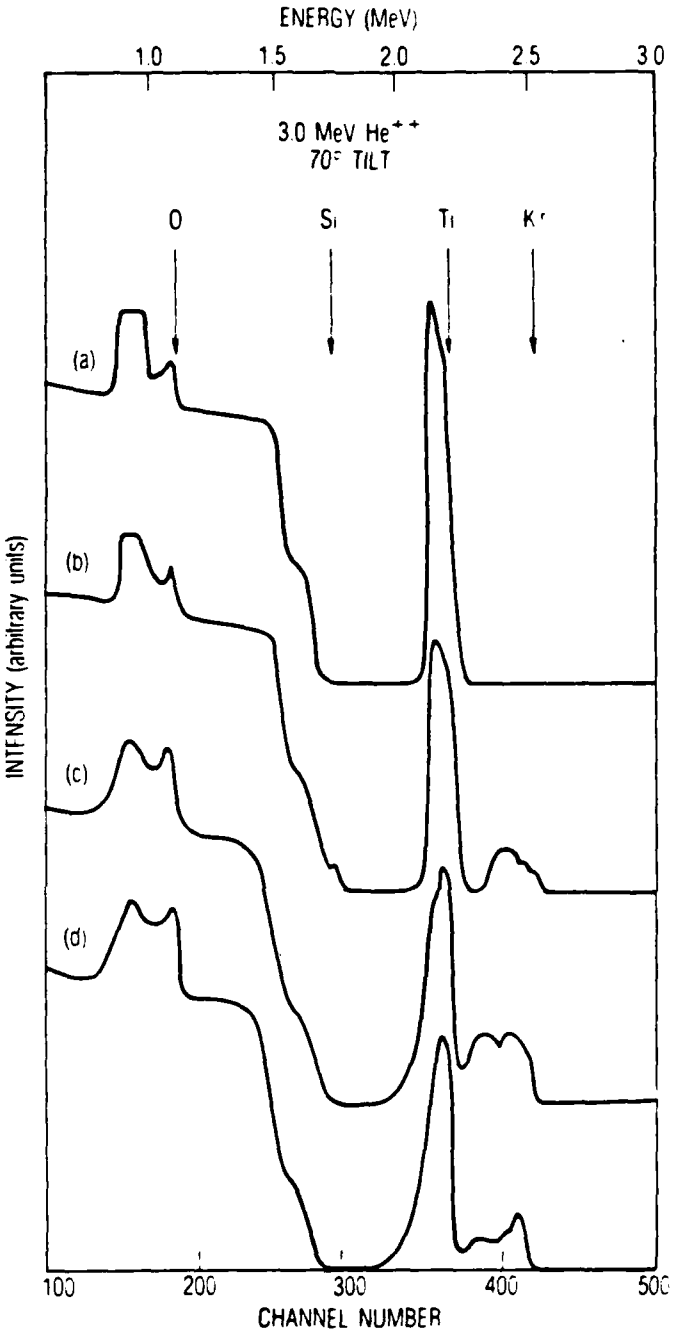

Fig. 3. RBS Spectra of $^{84}Kr^{+}$-Implanted Ti/SiO_x Specimens. (a) As-deposited specimen; (b) specimen implanted with 2×10^{16} Kr-cm^{-2} at 70°C; (c) specimen implanted with 1×10^{17} Kr-cm^{-2} at 70°C; (d) specimen implanted with 1×10^{17} Kr-cm^{-2} at 350°C.

The chemical bonding produced in these ion-mixed Ti/SiO_x specimens was examined using XRD and XPS analyses. As shown in Table 1, monoclinic TiO was the primary crystalline form produced by all of the $^{84}Kr^+$ implants. The specimens implanted with 1×10^{17} Kr-cm^{-2} gave additional diffraction lines corresponding to more highly oxidized crystalline forms (TiO_2 and Ti_3O_5). This increased oxidation and crystallization explains why the intermixed Si was expelled from the Ti films during high dose implantation. Si is insoluble in crystalline TiO_2.[13,17] Therefore, the solubility of Si in the Ti films decreased with ion-induced oxidation and crystallization. Any intermixed Si was driven out of the oxidized Ti films into the more highly disordered Ti-Si oxide films. The Kr content of the Ti films was also reduced as the films became more highly ordered.

Table 1. X-ray Diffraction Lines for Thermal and Ion-Processed Ti/SiO_x

As-deposited d(Å)/I	Vacuum Annealed d(Å)/I	2×10^{16} Kr-cm^{-2}, 70°C d(Å)/I	1×10^{17} Kr-cm^{-2}, 70°C d(Å)/I	1×10^{17} Kr-cm^{-2}, 350°C d(Å)/I
2.33/100[a]	3.57/8[c]	3.66/8[c]	3.59/20[c,d]	3.63/30[c,e]
2.24/50[b]	2.49/12[c]	3.47/8[c]	3.41/30[c]	3.31/90[c,e]
	2.38/12[c]	2.44/100[c]	2.38/30[c,d]	2.68/50[e]
	2.11/100[c]	2.07/50[c]	2.28/100[d]	2.04/100[c]
		1.48/20[c]	2.04/100[c,d]	1.68/30[c,e]
			1.49/12[c]	1.46/30[c]

[a]Hexagonal β-Ti, calculated.
[b]Hexagonal α-Ti, PDF #5-0682.
[c]Monoclinic TiO, PDF #23-1078.
[d]Tetragonal TiO_2 (anatase), PDF #21-1273.
[e]Monoclinic Ti_3O_5, PDF #11-217.

The mixed Ti-Si oxide layers produced in the $^{84}Kr^{+}$-implanted specimens were examined using XPS. XPS analyses performed after sputter erosion into the mixed oxide layer showed a single broad Si 2p peak at 102.6 eV, characteristic of partially oxidized silicon (~ SiO). Silicon monoxide is a non-crystalline metastable phase, which decomposes to form Si and SiO_2.[18,19] The presence of partially oxidized Si, rather than separate SiO_2 and Si phases, indicates that this Ti-Si oxide layer was a glassy mixture. Such a glass contains a high density of Si-O-Ti bonds.[13] The chemical state of the Ti in this mixed oxide layer could not be accurately determined by XPS analysis because of the chemistry modifications induced in titanium oxides by ion sputtering.

The adhesion between Ti and SiO_x in both the ion implanted and annealed Ti/SiO_x specimens was examined using a scratch test. The results of these scratch tests are summarized in Table 2. The adhesion values observed for the as-deposited, annealed, and ion-mixed specimens correlate with the extent of interfacial mixing and reaction (Si-O-Ti bond formation). The as-deposited Ti/SiO_x specimens had discrete interfaces, which showed little indication of reaction. These as-deposited films were weakly adherent, requiring only 5 g loads for removal. SEM/EDX analysis showed that the films were removed by brittle fracture at the Ti/SiO_x interface. We attribute this failure mode to stress concentration at the discrete Ti/SiO_x interfaces. An example of this

Table 2. Ti/SiO_x Scratch Tests

Sample Preparation	Load (g)	Sample Preparation	Load (g)
As-deposited	5[a]	2×10^{16} Kr-cm^{-2}, 70°C	15[b]
		1×10^{17} Kr-cm^{-2}, 70°C	50[b]
Vacuum Annealed	25[b]	1×10^{17} Kr-cm^{-2}, 350°C	50[b]

[a]Brittle interfacial fracture.
[b]Gradual thinning.

brittle interfacial failure is shown in Fig. 4a. The transfer of O into the Ti films, during thermal and low dose ion mixing, resulted in 3 to 5 fold adhesion increases. We attribute these adhesion increases to increases in Si-O-Ti bonding. The intermixing of the Ti and SiO_x layers by high-dose ion implantation further enhanced this Si-O-Ti bonding. This Ti-SiO_x intermixing increased film adhesion to 10 times that of the as-deposited specimens. As shown in Fig. 4b, film removal in the annealed and ion-mixed Ti/SiO_x specimens occurred through gradual thinning, rather than brittle interfacial failure. We attribute this change in failure mode to interfacial grading. The abrupt change in materials properties at a discrete interface promotes abrupt interfacial fracture under scratch testing. However, the gradual change in materials properties at a graded interface promotes interfacial deformation, rather than fracture. With a more gradual film removal mechanism, such thinning would be expected.

B. $TiO_y/SiO_x/Si$

The as-deposited TiO_y films were amorphous (examination by XRD) and smooth under SEM examination at 20,000X magnification. RBS analysis, presented in Fig. 5a, showed that the film stoichiometry was approximately TiO_3 and that the TiO_y/SiO_x interface was discrete. Vacuum annealing at 1000°C for 3600 s resulted in film crystallization to tetragonal TiO_2 (anatase). Grains 1 to 2 μm in diameter were observed under SEM examination. The RBS profile in Fig. 5b shows that vacuum annealing had no influence on the Ti and Si distributions. Crystalline TiO_2 and SiO_2 are immiscible.[13,17] However, oxygen, which is highly soluble (~ 30 atomic percent) in crystalline TiO_2 and SiO_2, migrated from the TiO_y layer to the Si/SiO_x interface, resulting in SiO_2 growth.

As-deposited TiO_y/SiO_x specimens were implanted with $^{84}Kr^+$ to 2×10^{16} Kr-cm^{-2} at 70°C, 1×10^{17} Kr-cm^{-2} at 70°C, and 1×10^{17} Kr-cm^{-2} at 350°C to determine the influence of ion dose and implantation temperature on specimen chemistry. The 2×10^{16} Kr-cm^{-2} implant had no influence on specimen topography or crystallinity. RBS analysis showed that the TiO_y/SiO_x interface had been slightly graded. A small quantity of Si (1.5 atomic percent) was mixed into the TiO_y layer.

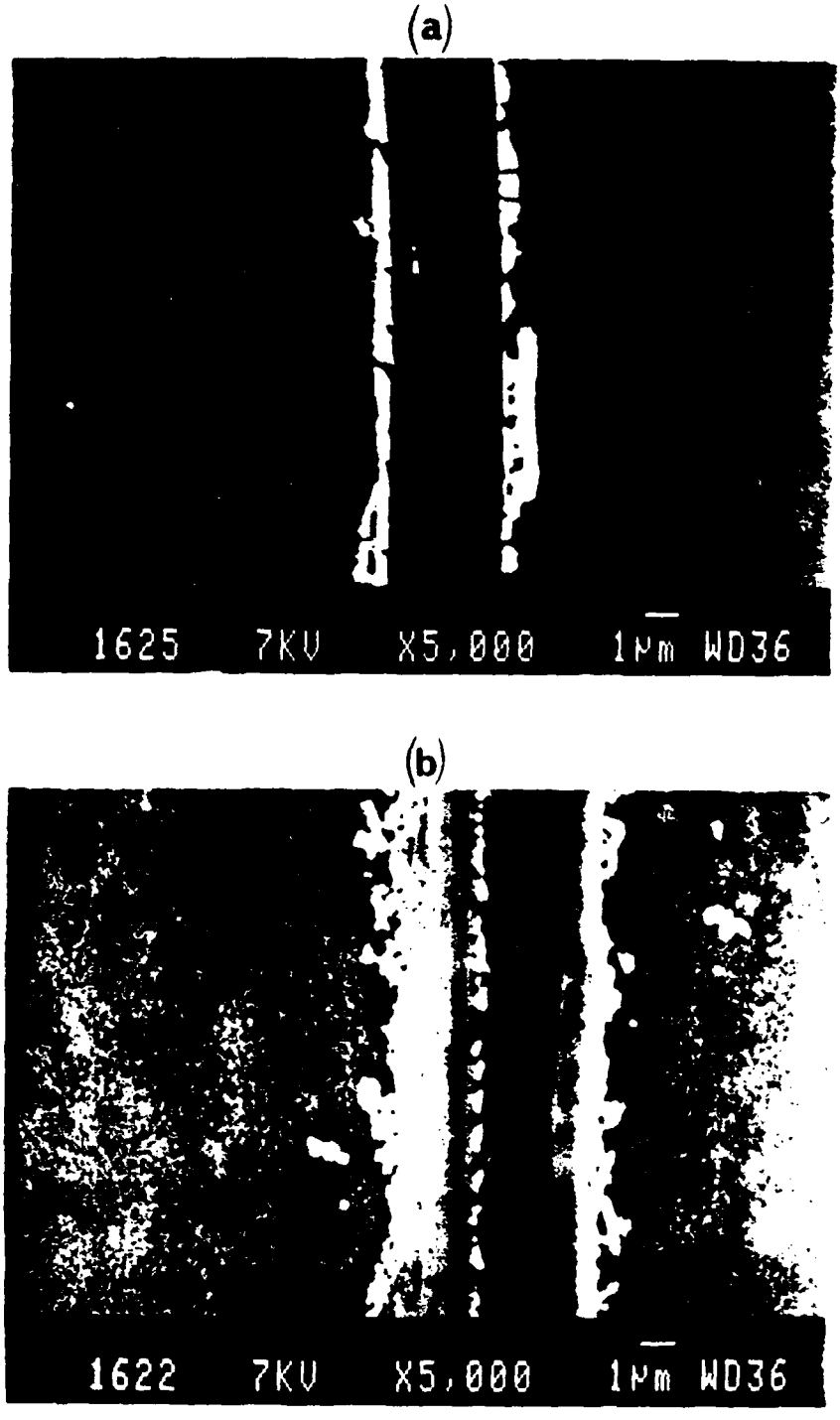

Fig. 4. SEM Micrographs of Scratches Performed on As-Deposited and Ion-Processed Ti/SiO_x Specimens. (a) 10 g scratch on as-deposited specimen; (b) 50 g scratch on specimen implanted with 1×10^{17} Kr-cm^{-2} at 70°C.

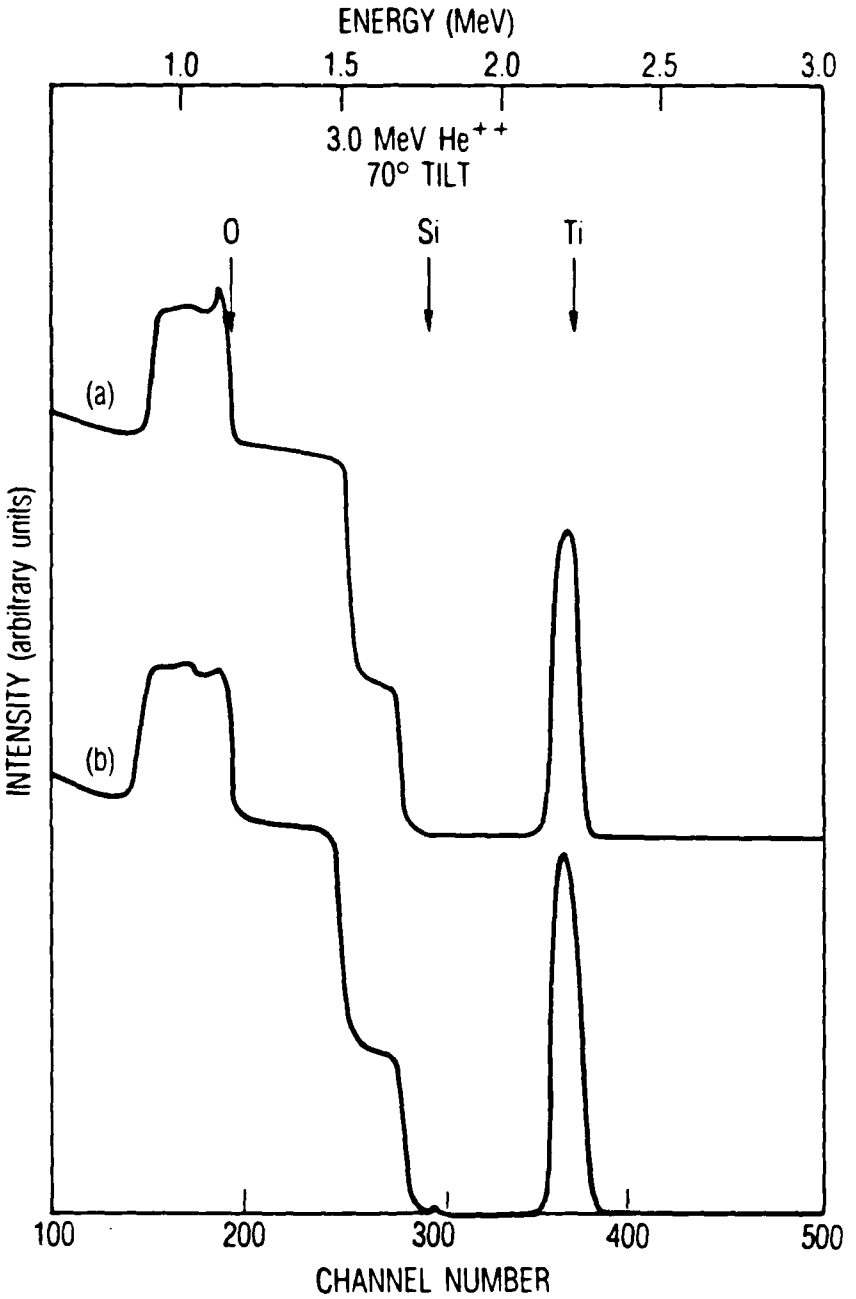

Fig. 5. RBS Spectra of As-Deposited and Annealed TiO_y/SiO_x Specimens. (a) As-deposited specimen; (b) Specimen vacuum annealed at 1000°C for 3600 s.

The 1×10^{17} Kr-cm^{-2} implants, performed at both 70 and 350°C, caused the TiO_y films to fracture into platelets 1 to 5 μm in diameter. The implanted Kr coalesced in the SiO_x films to form a high density of submicron-sized voids, resulting in film expansion. SiO_x expansion induced tensile stresses in the TiO_y films. The TiO_y films, which have much lower ductility than the Ti films, fractured under these tensile stresses, producing the platelet structure shown in Fig. 6. The voids produced by krypton coalescence are readily apparent in the cracks between the platelets, but are absent from the platelets.

AES depth profiles were obtained from the platelet and crack regions of these high-dose TiO_y/SiO_x specimens. Depth profiles performed in the platelet regions exhibited substantial grading at the TiO_y/SiO_x interface, much like

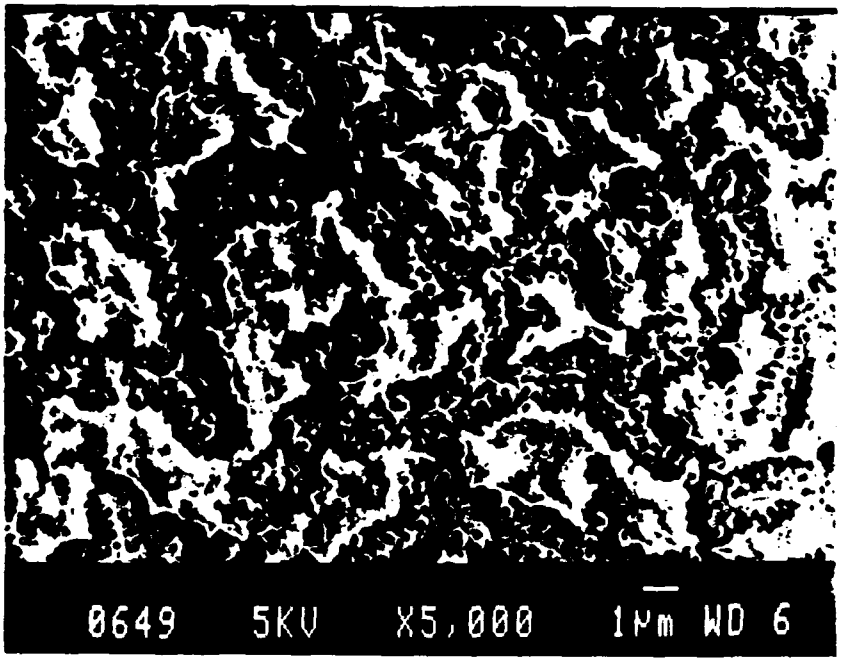

Fig. 6. SEM Micrograph of a TiO_y/SiO_x Specimen, Following Implantation with 1×10^{17} Kr-cm^{-2} at 70°C. The surface, which was initially smooth, was transformed into a series of cracks and platelets. A high density of voids is observed in the crack regions.

that observed in the ion-mixed Ti/SiO_x specimens. The quantity of Ti mixed into the SiO_x layers increased with ion dose and temperature, but the quantity of Si in the TiO_y layers decreased with ion dose and temperature. The interfacial mixing induced by the 1×10^{17} Kr-cm^{-2} implant performed at 350°C is shown in Fig. 7b. The Ti distribution extends completely through the SiO_x layer. The Si distribution extends partially into the TiO_y, but leaves most of the TiO_y film intact. Depth profiles (Fig. 7c) obtained from the crack regions did not exhibit this TiO_y layer. The cracks were composed of an intermixed layer of Ti, Si, and O, which was graded into the Si substrate. This mixed composition verified that the cracks had originated from the intermixed TiO_y/SiO_x interface.

The chemistry of these ion-mixed TiO_y/SiO_x specimens was examined using XRD and XPS analyses. The X-ray diffraction patterns (presented in Table 3), obtained from the specimens implanted with high $^{84}Kr^+$ doses, showed that the TiO_y surfaces had crystallized to tetragonal TiO_2 (both rutile and anatase). The absence of any reduced crystalline forms (TiO, Ti_2O_3, etc.) indicates that the TiO_y film had crystallized with a high degree of perfection. As with the ion-mixed Ti/SiO_x specimens, this crystallization forced defects (such as intermixed Si and coalesced Kr) out of the TiO_2 films. The absence of partially oxidized crystalline forms also indicates that the Ti in the Ti-Si oxide layer had one distinct form. It was present in either a glassy mixture (no diffraction pattern) or in a crystalline TiO_2 phase. XPS spectra taken from these mixed oxide layers exhibited a single Si 2p peak at 103.3 eV, characteristic of SiO_2. Such a peak would be observed from a separate SiO_2 phase or a glassy mixture of SiO_2 and TiO_2. It is unclear from the XRD and XPS analyses whether the intermixed region was composed of a glassy mixture, or separate SiO_2 and TiO_2 phases.

The results of adhesion tests performed on the as-deposited, annealed, and ion processed TiO_y/SiO_x specimens are summarized in Table 4. Ion mixing and annealing produced only small changes in the adhesion of the TiO_y films. The as-deposited films were removed at 25 g loads. Annealing at 1000°C for 3600 s reduced this critical load to 17 g. Film crystallization either increased the intrinsic stress at the interface, or enhanced the transfer of

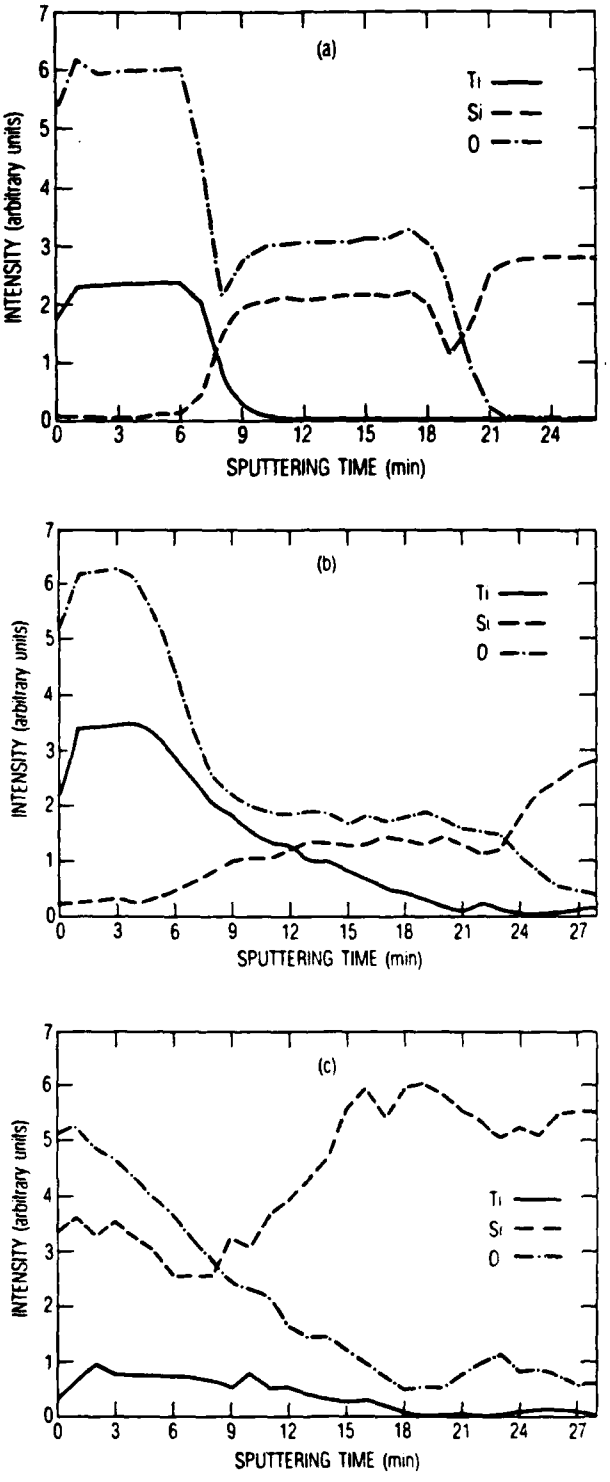

Fig. 7. AES Depth Profiles of TiO_y/SiO_x Specimens Before and After Implantation with 1×10^{17} Kr-cm^{-2} at 350°C. (a) As-deposited specimen; (b) Surface platelet on the implanted specimen; (c) Crack region between platelets on the implanted specimen.

Table 3. X-ray Diffraction Lines for Thermal and Ion-Processed TiO_y/SiO_x

As-deposited d(Å)/I	Vacuum Annealed d(Å)/I	2×10^{16} Kr-cm^{-2}, 70°C d(Å)/I	1×10^{17} Kr-cm^{-2}, 70°C d(Å)/I	1×10^{17} Kr-cm^{-2}, 350°C d(Å)/I
No Lines Observed	3.65/100[a]	No Lines Observed	3.66/8[a]	3.21/100[b]
	2.48/20[a,b]		3.22/100[b]	2.50/30[a,b]
	1.97/20[a]		2.30/8[b]	1.69/30[b]
	1.76/20[a]			

[a]Tetragonal TiO_2 (anatase), PDF #21-1273.
[b]Tetragonal TiO_2 (rutile), PDF #21-1276.

Table 4. TiO_y/SiO_x Scratch Tests

Sample Preparation	Load (g)	Sample Preparation	Load (g)
As-deposited	25[a]	2×10^{16} Kr-cm^{-2}, 70°C	10[b]
		1×10^{17} Kr-cm^{-2}, 70°C	30[b]
Vacuum Annealed	17[a]	1×10^{17} Kr-cm^{-2}, 350°C	30[b]

[a]Brittle interfacial fracture.
[b]Gradual thinning.

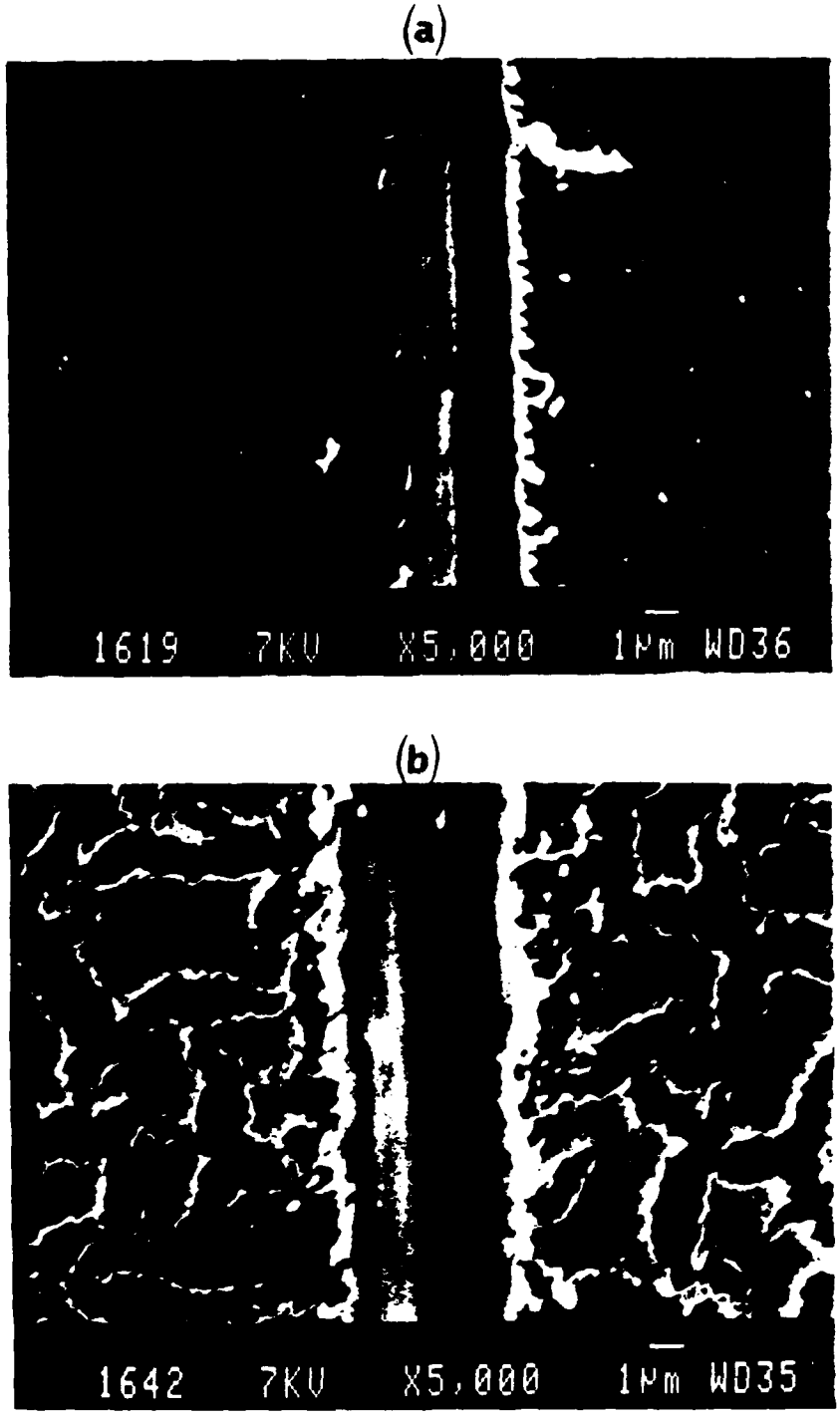

Fig. 8. SEM Micrographs of Scratches Performed on Thermal and Ion-Processed TiO_y/SiO_x Specimens. (a) 17 g scratch on specimen annealed at 1000°C for 3600 s; (b) 30 g scratch on specimen implanted with 1×10^{17} Kr-cm^{-2} at 70°C.

applied stress to the interface. Both the as-deposited and annealed TiO_y films were removed through brittle interfacial fracture that resulted from stress concentration at the discrete TiO_y/SiO_x interfaces. An SEM micrograph of the brittle fracture induced by a 17 g scratch on a vacuum annealed TiO_y/SiO_x specimen is shown in Fig. 8a. The TiO_y films implanted with 2×10^{16} Kr-cm^{-2} showed a reduction in adhesion to 10 g loads. Apparently, the interfacial stresses induced by ion implantation (SiO_x expansion) were far greater than any adhesion enhancement. For those specimens implanted with 1×10^{17} Kr-cm^{-2}, ion-induced interfacial stresses were relieved by the fracturing of the TiO_y films. The loads required to remove these high-dose films remained approximately the same as the as-deposited films. As shown in Fig. 8b, the $^{84}Kr^+$ implanted films were not removed by interfacial fracture, but were removed through a gradual thinning process. The gradual change in materials properties at the graded (ion-mixed) TiO_y/SiO_x interfaces promotes interfacial deformation, rather than fracture.

Although the TiO_y and SiO_x films were mechanically interlocked through ion mixing, the adhesion of the TiO_y films was not improved. Apparently, interfacial mixing was not accompanied by enhanced Si-O-Ti bonding across the TiO_y/SiO_x interface. The XRD data obtained from the ion mixed TiO_y/SiO_x specimens indicated that the form of the Ti in the mixed oxide layer was either glassy (extensive Si-O-Ti bonding) or highly crystalline (little Si-O-Ti bonding). We attribute the absence of ion-induced adhesion enhancement to TiO_2 crystallization and phase separation in the interfacial Ti-Si oxide layer. However, a further investigation, including high energy electron diffraction, is required to verify this hypothesis.

IV. SUMMARY/CONCLUSIONS

Ion implantation induced interfacial mixing at both the TiO_y/SiO_x and the Ti/SiO_x interfaces. As with thermal processing, ion implantation enhanced the reduction-oxidation reaction between the Ti and SiO_x layers, resulting in O redistribution into the Ti films. Contrary to thermal processing, ion implantation induced the redistribution of Ti from the Ti and TiO_y films into the underlying SiO_x layers. Silicon was also ion mixed into the Ti and TiO_y films, but most of this intermixed Si was expelled because of the poor solubility of Si in crystalline TiO_2. Ion-induced interfacial mixing, which produced interfacial Ti-Si oxide layers in both the Ti/SiO_x and TiO_y/SiO_x specimens, increased with ion dose and implantation temperature.

Although ion implantation induced similar interfacial mixing in both the TiO_y/SiO_x and Ti/SiO_x specimens, ion implantation had a very different influence on the adhesion of the Ti and TiO_y films. The interfacial mixing (mechanical interlocking) induced by ion implantation enhanced the adhesion of the Ti films by 10-fold, but did not enhance the adhesion of the TiO_y films. The observed adhesion increases were attributed to increased Si-O-Ti bonding. Because of the low O content of the Ti films, interfacial mixing in the Ti/SiO_2 specimens inevitably produced greater Si-O-Ti bonding (adhesion enhancement). This was not true in the TiO_y/SiO_x specimens. In fact, XRD analyses indicate that the mixed Ti-Si oxide layers in the TiO_y/SiO_x specimens may have separated into discrete TiO_2 and SiO_2 phases.

The topography of the Ti and TiO_y films was also influenced differently by ion implantation. The coalescence of the implanted Kr induced SiO_x expansion. This expansion induced tensile stresses in both the Ti and TiO_y films. These stresses caused the brittle TiO_y films to fracture into platelets. The Ti films, which have greater ductility than the TiO_y films, did not fracture, but showed signs of plastic deformation.

From this investigation, it is clear that both metal/oxide and oxide/oxide interfaces may be mixed rather extensively by ion implantation. However, this interfacial mixing does not necessarily enhance adhesion. Increased chemical bonding across the interface is required for adhesion

improvement. As with the TiO_y/SiO_x specimens, this chemical bonding may not be observed between oxide layers that are not thermodynamically reactive. In addition, the high implantation doses required to intermix an oxide/oxide interface can result in substantial topographical damage, which is unacceptable for most thin film applications.

REFERENCES

1. I. L. Singer, Appl. Surf. Sci. 18, 28 (1984).

2. M. Van Rossum, M-A. Nicolet, and C. H. Wilts, J. Appl. Phys. 56, 1032 (1984).

3. K. C. Cadien and J. E. Greene, Appl. Phys. Lett. 40, 329 (1982).

4. J. W. Mayer and S. S. Lau, "Surface Modification and Alloying by Laser, Ion, and Electron Beams," edited by J. M. Poate, G. Foti, and D. C. Jacobson (Plenum, New York, 1983), p. 240.

5. S. Matteson and M-A. Nicolet, Ann. Rev. Mater. Sci. 13, 339 (1983).

6 A. A. Galuska, J. Vac. Sci. Technol. B 5, 1 (1987).

7. D. M. Mattox, "Adhesion Measurement of Thin Films, Thick Films, and Bulk Coatings," edited by K. L. Mittal (American Society for Testing and Materials, Philadelphia, 1978), p. 54.

8. I. V. Mitchell, J. S. Williams, D. K. Sood, K. T. Short, S. Johnson, and R. G. Elliman, in "Proceedings of MRS Symposium on Thin Films and Interfaces," edited by J. E. E. Baglin, D. R. Campbell, and W. K. Chu (North Holland, New York, 1984), p. 189.

9. J. E. E. Baglin and G. J. Clark, Nucl. Instrum. Methods Phys. Res. B 107, 89 (1985).

10. S. Jacobson, B. Johnson and B. Sunquist, Thin Solid Films 107, 89 (1983).

11. C. W. White, G. Farlow, J. Narayan, G. J. Clark, and J. E. E. Baglin, Mat. Lett. 2, 367 (1984).

12. T. A. Tombrello, "Proceedings of MRS Symposium on Thin Films and Interfaces," edited by J. E. E. Baglin, D. R. Campbell, and W. K. Chu (North-Holland, New York, 1984), p. 179.

13. M. F. Best and R. A. Condrate, J. Mat. Sci. Lett. 4, 994 (1985).

14. R. Kelly, "Ion Bombardment Modification of Surfaces," edited by O. Auciello and R. Kelly (Elsevier, New York, 1984), p. 85.

15. I. S. Goldstein and R. DeLong, J. Vac. Sci. Technol. 20, 327 (1982).

16. B. N. Chapman, J. Vac. Sci. Technol. 11, 106 (1947).

17. R. C. De Vries, R. Roy and E. F. Osborn, Trans. Brit. Ceram. Soc. 53, 531 (1954).

18. R. B. Sosman, Trans. Brit. Ceram. Soc. 54, 655 (1955).

19. H. H. Emons and H. Boenicke, Wess. Z. Tech. Hochsch. Chem. Leuna-Merseburg 4, 115 (1961).

LABORATORY OPERATIONS

The Aerospace Corporation functions as an "architect-engineer" for national security projects, specializing in advanced military space systems. Providing research support, the corporation's Laboratory Operations conducts experimental and theoretical investigations that focus on the application of scientific and technical advances to such systems. Vital to the success of these investigations is the technical staff's wide-ranging expertise and its ability to stay current with new developments. This expertise is enhanced by a research program aimed at dealing with the many problems associated with rapidly evolving space systems. Contributing their capabilities to the research effort are these individual laboratories:

Aerophysics Laboratory: Launch vehicle and reentry fluid mechanics, heat transfer and flight dynamics; chemical and electric propulsion, propellant chemistry, chemical dynamics, environmental chemistry, trace detection; spacecraft structural mechanics, contamination, thermal and structural control; high temperature thermomechanics, gas kinetics and radiation; cw and pulsed chemical and excimer laser development including chemical kinetics, spectroscopy, optical resonators, beam control, atmospheric propagation, laser effects and countermeasures.

Chemistry and Physics Laboratory: Atmospheric chemical reactions, atmospheric optics, light scattering, state-specific chemical reactions and radiative signatures of missile plumes, sensor out-of-field-of-view rejection, applied laser spectroscopy, laser chemistry, laser optoelectronics, solar cell physics, battery electrochemistry, space vacuum and radiation effects on materials, lubrication and surface phenomena, thermionic emission, photosensitive materials and detectors, atomic frequency standards, and environmental chemistry.

Computer Science Laboratory: Program verification, program translation, performance-sensitive system design, distributed architectures for spaceborne computers, fault-tolerant computer systems, artificial intelligence, microelectronics applications, communication protocols, and computer security.

Electronics Research Laboratory: Microelectronics, solid-state device physics, compound semiconductors, radiation hardening; electro-optics, quantum electronics, solid-state lasers, optical propagation and communications; microwave semiconductor devices, microwave/millimeter wave measurements, diagnostics and radiometry, microwave/millimeter wave thermionic devices; atomic time and frequency standards; antennas, rf systems, electromagnetic propagation phenomena, space communication systems.

Materials Sciences Laboratory: Development of new materials: metals, alloys, ceramics, polymers and their composites, and new forms of carbon; nondestructive evaluation, component failure analysis and reliability; fracture mechanics and stress corrosion; analysis and evaluation of materials at cryogenic and elevated temperatures as well as in space and enemy-induced environments.

Space Sciences Laboratory: Magnetospheric, auroral and cosmic ray physics, wave-particle interactions, magnetospheric plasma waves; atmospheric and ionospheric physics, density and composition of the upper atmosphere, remote sensing using atmospheric radiation; solar physics, infrared astronomy, infrared signature analysis; effects of solar activity, magnetic storms and nuclear explosions on the earth's atmosphere, ionosphere and magnetosphere; effects of electromagnetic and particulate radiations on space systems; space instrumentation.

...